SPAWAR

**Systems Center
PACIFIC**

Silicon Carbide Defect Qubits/Quantum Memory with Field-tuning: OSD Quantum Science and Engineering Program (QSEP)

Osama Nayfeh
Brad Liu
Vincent Dinh
Carlos Torres
Mark Lasher
Anna Leese de Escobar
Bradley Davidson
Patrick Sims
Sanja Zlatanovic
Brian Higa
SSC Pacific

Lance Lerum
Hector Romero
**Naval Research Enterprise
Internship Program**

Mohammed Fahem
**San Diego State University
Research Foundation**

Hunter Banks
Sam G. Carter
D. Kurt Gaskill
Thomas L. Reinecke
Naval Research Laboratory

SSC Pacific
San Diego, CA 92152-5001

The citation of trade names and names of names of manufacturers is not to be construed as official government endorsement or approval of commercial products or services referenced in this report.

Horiba^{TM} iHR320 imaging spectrometer is a product of Horiba Instruments Incorporated.
Hamamatsu is a trademark of Hamamatsu Photonics Inc.
MATLAB$^{®}$ is a registered trademark of The MathWorks.

SB

EXECUTIVE SUMMARY

Collaboration between Space and Naval Warfare Systems Center Pacific (SSC Pacific) and National Research Laboratory (NRL) was initiated in 2015 and 2016 as part of the Office of the Secretary of Defense (OSD) Quantum Science and Engineering Program (QSEP). Their collaboration topic was to examine the effect of electric-field on silicon carbide qubits as a unique contribution as well as general benefit in increasing knowledge in the quantum information field by SSC Pacific personnel and working towards supporting demonstrations of quantum entanglement based on these qubits and quantum memories developed out of the silicon carbide system and other systems as necessary through the QSEP program. During this year, highlights included successful completion of a novel process flow for the construction of the tunable qubits, measurements of the optical emission from the devices, and simulations of the tuning process as well as upgrade in progress for experimental validation of the concepts and towards supporting entanglement demonstrations. A patent disclosure was filed on the concept of tunable silicon carbide qubits as well as a conference abstract was submitted to the SPIE 2017 Nanoscience + Engineering Conference for Consideration in the Quantum Photonic Devices Section. This work is funded by the Office of the Secretary of Defense Quantum Science and Engineering Program

CONTENTS

Figures

Tables

1. INTRODUCTION AND QUANTUM NETWORKS

The Office of Secretary of Defense launched a large program to establish the first U.S.-based quantum network. Quantum networks are based on quantum entangled quantum qubits/memories. We expect that such networks would provide increased security over conventional networks, as well as provide complimentary capability for improved sensing and enable concepts such as distributed quantum computing. Success requires research and development (R&D) into the qubits and quantum memories (devices that can process quantum information states |0> and |1> and store them for sufficient time to implement a quantum computation or communication, etc. Additionally, the ability to send the quantum entangled states is important, so advances in enabling photonic technologies, preferably on-chip, are required. Figure 1 shows the overall QSEP program schedule.

	FY16	FY17	FY18	FY19
SiC-based memory	NRL/ARL: Fab, interface, demo memory		entangle spins	
Integrated photonics	AFRL: Design → fab →demo			
Ion-based memory	AFRL/ARL: Fab, interface, demo memory		demo freq. conv.	
Vacuum cells	ARL: Design → build			
UV Lasers/ Detectors	ARL: Material growth → processing → device characterization			
Universal controller	ARL: Build FPGA hardware → develop software → integrate			
Two-node quantum network				Entangle 2 nodes & demo sensor app.
Sensors	AFRL, NAVAIR, AMRDEC: Integrate on-chip wires/waveguides onto atom sensor		down-select	
	NRL: Demonstrate sensing with solid-state platform		Demo high-sensitivity prototype sensor	
Quantum sensor network design	ARL, AFRL, NRL: Develop sensor network model; validate/ compare protocols to map sensor info onto network		Develop software tools & prototype secure protocols	

Figure 1. Overall QSEP program schedule.

In particular, in this work we examine defect qubits in silicon carbide, as they are an emerging system for quantum information science and technology that can produce in the solid state. It is important to passivate and protect the surface to preserve the particular defect configurations, as well as provide means to tune the opto-electronic properties via electronic or opto-electronic gating. In this work, we construct defect qubit device structures that integrate indium-tin-oxide (ITO) electrodes and a thin atomic layer deposited (ALD) silicon-oxide surface passivation. The devices are formed through ^{12}C ion implantation and high-temperature annealing of 4H and 6H silicon carbide. The process involves the integration of optically transparent indium tin oxide electrodes and a surface passivation film of silicon-oxide by atomic layer deposition. We find good contact is formed between ITO and SiC, and after complete processing, the measured broad-band photoluminescence (PL) with excitation at 785-nm in a scanning PL system is consistent with the formation of silicon vacancies. We find minimal change in the room temperature emission in regions beneath the ITO electrodes and the SiO_x-SiC passivated surface. We evaluate the ability of electric field to tune the optically detected magnetic resonance (ODMR) response of the qubit system by simulations of the

spectrum with a modified spin Hamiltonian that considers the Stark Effect. We quantify the simulated strength of the electric-field tuning of the energy levels and ODMR response for the various identified spin 3/2 transitions of the silicon vacancy.

2. PROJECT SCHEDULE (THIS WORK)

A project schedule was developed to meet the project objectives as described in Figure 1 is shown in Figure 2.
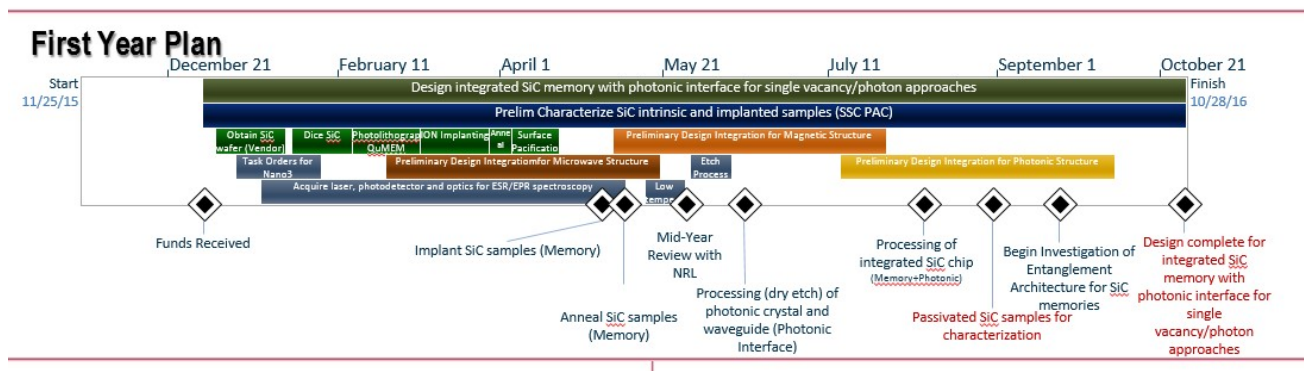
Figure 2. Project schedule for collaborative effort.

3. PROCUREMENTS AND CONTRACT ACTIONS

The following materials and contract actions were completed as part of this effort.

1. Procurement of silicon carbide wafers
   a. 4H SiC (Cree™, Inc.)
   b. 6H SiC (II-VI, Inc.)
2. Procurement of dicing service (American Precision)
3. Procurement of an ion implant service (Innovion Corporation)
4. Procurement of a 976-nm solid-state fiber-optic laser (ThorLabs Inc.)
5. Procurement of a vacuum storage chamber (Pelco)
6. Procurement of a mask set for construction of the devices (Photo Sciences)
7. Procurement of an equipment rack
8. Procurement of an optical spectrum analyzer (OSA) (Yokogawa)
9. Contract action for access to Nano3 facility at UC San Diego
   a. Cleanroom access
   b. Special equipment
   c. Analytical labs
10. Task order contract action for student support through the San Diego State University Research Foundation (SDSURF) Program

11. Procurement of Laser Systems

    a. 532-nm 40-mW solid-state laser

    b. 808-nm 1-W laser diode

    c. 850-nm 30-mW laser diode

    d. Laser diode mount with thermoelectric coooling (TEC) built-in and accessories for mounting

    e. Laser power supply

    f. TEC power supply

12. Optical filters from SEMROCK®, THORLABS Inc., EDMUND OPTICS®

    a. 532-nm, laser-line filter (SEMROCK®)

    b. 550-nm, hard-coated, short-pass filter (THORLABS Inc.)

    c. 532-nm long-pass filter (SEMROCK®)

    d. 808-nm laser-line filter (SEMROCK®)

    e. 850-nm /10-nm full width at half maximum (FWHM) bandpass filter (SEMROCK®)

    f. 980-nm bandpass filter (SEMROCK®)

    g. 976-nm laser-line pass filter (SEMROCK®)

    h. 850-nm long-pass filter (EDMUND OPTICS® x2)

13. Laser safety items and satisfying on-site requirements

    a. Laser barrier panels x2

    b. Laser goggles appropriate for the aforementioned wavelengths x2

    c. Laser operation light sign

14. Opto-mechanics and tools

    a. Optical Post Kit (THORLABS Inc.)

    b. Optical Post Base Plate Kit (THORLABS Inc.)

    c. Optical Post Holder Kit (THORLABS Inc.)

    d. Optical fiber cleaner and related items (THORLABS Inc.)

    e. Optical fiber connector adapters for LC/FC, Advanced Power Control (APC), and FC/SMA APC FIBERTRONICS and THORLABS Inc.

    f. Lenses and mirrors (THORLABS Inc.)

    g. Tools such as screwdrivers and various adapter spanner wrenches (THORLABS Inc.)

    h. Optical power meter (THORLABS Inc.)

    i. Monochrome Configuration Memory Operating System (CMOS) Si Camera and Lens System (THORLABS Inc.)

15. Tesla Meter (PASCO®)

16. In addition to these procurements, we are leveraging an in-house capital funds investment to procure a cryo magneto-optical probe station.

4. CONCEPT OF TUNABLE QUBITS

4.1 VACANCIES/DEFECT QUBITS IN SILICON-CARBIDE

A qubit is a two-level system that can be based on atoms, ions, quantum dots, or even defects in crystals. The difference between these two-level systems and those based on classical objects are that they obey quantum mechanics, and thus can permit quantum physics operations, such as tunneling and entanglement on these two levels that effectively comprise quantum information states |0> and |1>. The interesting thing about using defects in crystals for qubits is that they can be constructed using micro-nanofabrication techniques and can benefit from many of the advantages of high-tech electronics such as scalability, low cost, large-scale integration, compatibility with supporting components, etc. A few types of solid-state qubits are being investigated worldwide and these include nitrogen vacancies in diamond, dopants in silicon, vacancies in silicon carbide, and rare-earth ions in crystals. Regardless of the type of system used, the "atom-like" element must meet certain criteria for use as a qubit. As this collaboration centers on the use of silicon carbide for various technological reasons, as well as meeting these criteria, we will discuss these factors here. Vacancy defects in silicon-carbide are being pursued for use as qubits due to meeting several criteria, specifically regarding spin states that can be controlled (i.e., rotated and flipped) with substantial quantum coherence time of these spin states through optical and microwave excitation, a kind of hybrid process that combines concepts from nuclear/electronic magnetic resonance and spintronic that can be implemented in the solid-state with atom-like defects in a host crystal. Figure 3 shows the lattice structure for 4H-SiC and 6H-SiC. Figure 4 shows calculated energy levels verses the magnetic field.
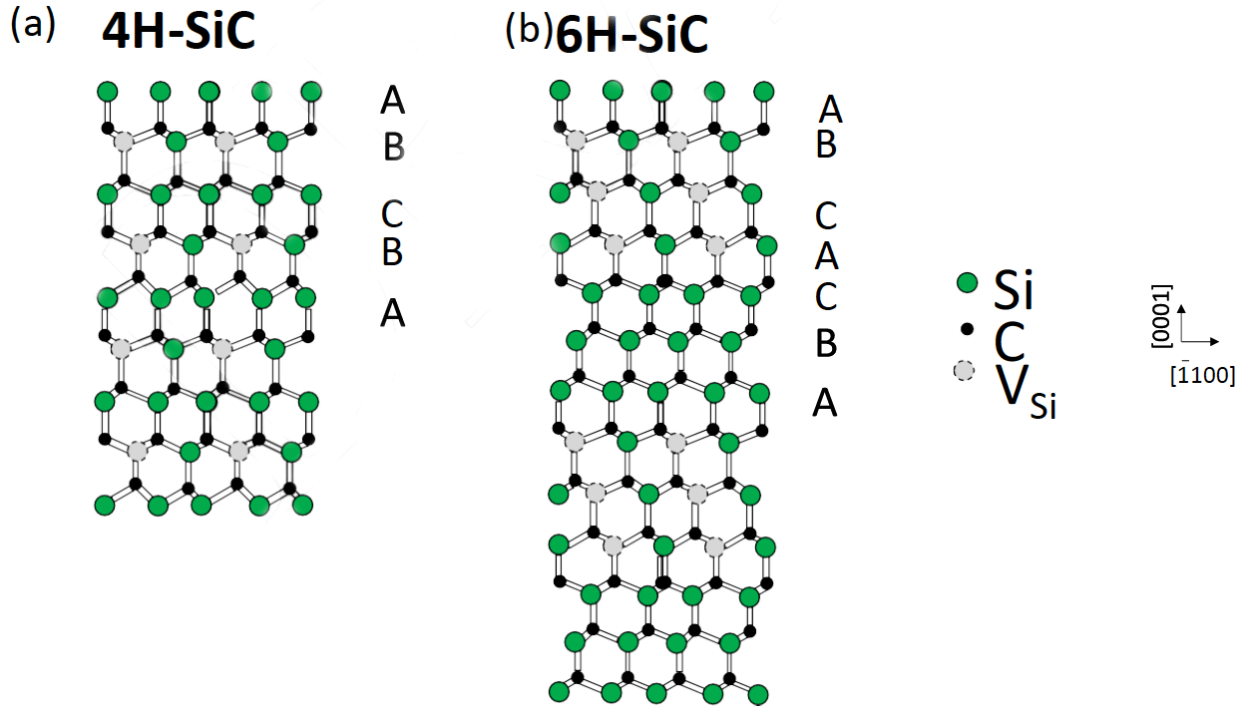
Figure 3. (a) Lattice structure for 4H-SiC with ABCBA periodicity and 6H-SiC with ABCACBA periodicity.

Shown are the Si, C and Si vacancies which are the focus of this work. Please keep in mind that due to non-ideality in the fabrication process other defects likely exist.

Figure 4 shows calculated energy leves versus magnetic field with and without an additional electric field. Six tranditios a-f, have been idemntified basaed on what is possible according to quantum mrvhanics.
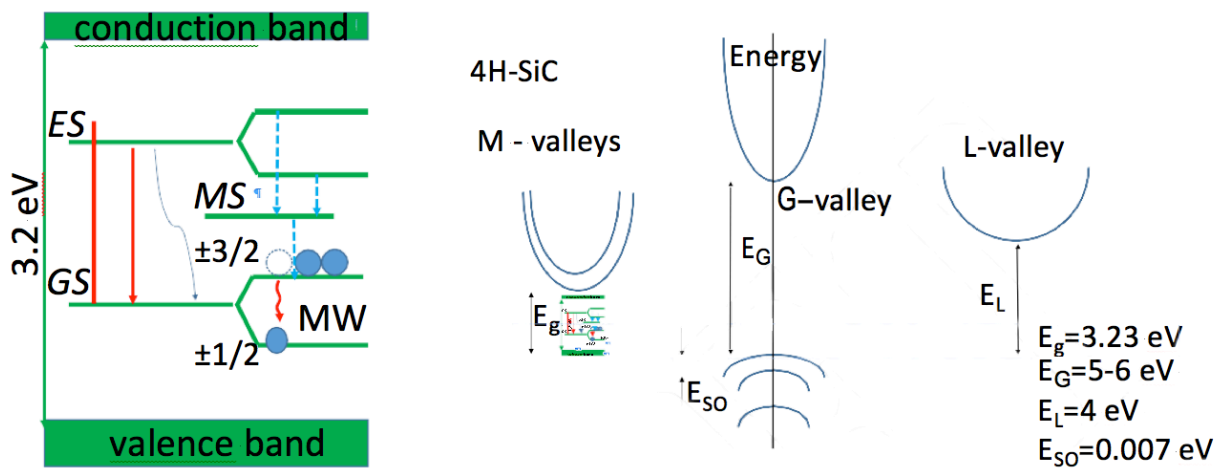
Figure 4. Calculated energy levels vs. magnetic field.

According to recent density functional theory and experimental validation analysis, the physical effects behind a possible electric field tuning captured through an effective Stark-like effect of the qubit response is due largely to a combination of distortion of the atomic/ionic lattice as well as direct field-induced shifts of the wave functions, where the latter is expected to be greater. Owing to the high polarizability with dielectric constant of ~10 of SiC, the effects can be quite substantial and even stronger than that of diamond crystals.

4.2 SPIN HAMILTONIAN SIMULATIONS OF EFFECT OF FIELD-EFFECT TUNINING

To understand the operation of the qubits and to quantify the anticipated tuning of the qubit properties, we employed a spin Hamiltonian model and modified it to include a term in the Hamiltonian corresponding to electric field. The objective is to recalculate the effect of electric field on the energy levels and resulting optically detected magnetic resonance (ODMR) spectra, to search for possibility of tuning the ODMR or even discovery of potential for new transitions if significant perturbation of the energy levels is expected. The Hamiltonian considered without electric field as reported in (Carter et al., 2015) is

$$H = g\mu_B \vec{B} \cdot \vec{S} + DS_z^2 + H_{hf},$$

where $g=$ is the electron g factor, μ_B is the Bohr magneton, $\vec{B}$ is the magnetic field, $2D$ is the zero-magnetic field splitting parameter, $\vec{S}$ is the vector of spin 3/2, and H_{hf} is considering the hyperfine interaction between the next nearest neighbor (NNN)[29] Si nuclear spin and the silicon vacancy (defect) spin. Looking at the full lattice description and full band-structure, it is possible that other factor contribute to the overall response of the material, but for the atom-like description and the regime of excitation these elements are the primary factors of interest to the Hamiltonian in this analysis in describing the system and the elements that can be engineered. Further details on the model can be found in Carter et al. (2015).

In this work, we introduce an additional term to consider, the effect of electric field, and examine the impact on the energy levels as a function of magnetic field as well as the calculated ODMR spectra. We base this approach on the recent work of Falk et al.,2014 so the modified Hamiltonian becomes, with the H_{hf} term expanded to include electric field matrices,

$$H = g\mu_B \vec{B} \cdot \vec{S} + DS_z^2 + \left(H_{hf} - E_x(\sigma_x^2 - \sigma_y^2) + E_y(\sigma_x\sigma_y + \sigma_y\sigma_x) \right).$$

Figure 4 shows calculated energy levels versus magnetic field with and without an additional electric field. Six transitions a–f have been identified based on what is possible according to quantum mechanics for the spin 3/2 defects. Figure 5 presents simulations of the ODMR spectra also with and without an electric field. It is promising that significant sensitivity in the ODMR spectra is observable nominal electric fields that would be readily resolvable in an experiment. Figure 5 shows an example of Silicon Vacancy (spin 3/2) ODMR simulations with E-Field (a–f) transitions.

Example of Silicon Vacancy (spin 3/2) ODMR Simulations with E-Field (a–f) transitions
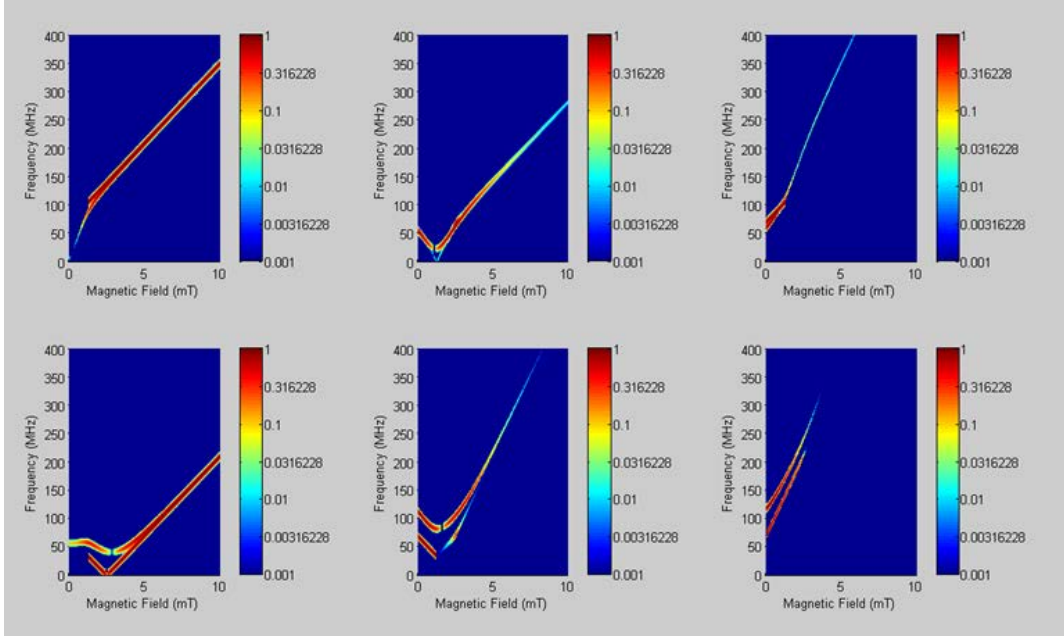

Figure 5. ODMR simulations of the identified a–f spin 3/2 transitions with and without a nominal electric field applied demonstrating.

5. QUBIT/QUANTUM MEMORY DEVICE DESIGN AND FABRICATION

5.1 DEVICE DESIGN CONSIDERATIONS

We developed a novel process for the construction of the devices. The process addresses four things: (1) the need to passivate the surface to protect the vacancy configuration, (2) integrate contacts that are optically transparent so that the qubit can be excited and the optical emission detectable from the regions beneath the contacts, (3) implementation of a layout where microwave power can be inputted at frequencies commensurate with the driving frequencies for the energy level of the transitions of the qubit system, and (4) ability to apply electric field in the c-axis direction (i.e. between contact and bottom of wafer) as well as in two-dimensions, i.e., in the channel region between contacts.

5.2 DEVICE FABRICATION PROCESS

Starting materials are 4" 4 and 6H purity semi-insulating silicon carbide, as well as 4" silicon control wafers for comparison. The 4H SiC is procured from Cree Inc. and the 6H SiC from II-VI Inc. and the silicon wafers from university wafer. Figure 6(a) shows a picture of a typical wafer before dicing. The wafers were sent for dicing service and were diced into 19.5- x 19.5-mm squares. The size of the pieces is selected to provide sufficient material for the varied experimental conditions encountered in this study, as well as compatibility with the thermal annealing furnace used in the process. The source must be large enough to ensure that a device nears the center of the sample are minimally impacted by human wafer handling in the clean-room.
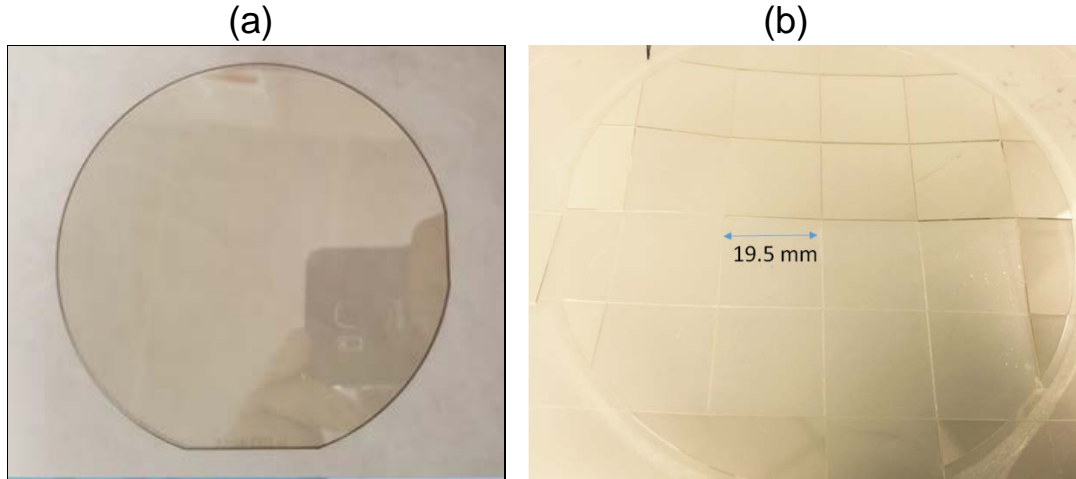
Figure 6. (a) 4" silicon carbide wafer before dicing

After dicing, 8 nm of SiOx were deposited by atomic layer deposition to serve as an implant and annealing cap. The ALD was performed in a class 100 clean room using the Nano3 facilities at UC San Diego and based on standard recipes using water and (x) precursors at 200 °C. A standard procedure in the literature for producing defects are by ion implantation with ^{12}C and subsequent high temperature annealing with 900 to 1000 °C temperatures. Typical doses range from 10^{11} to 10^{13} ions/cm^2 and energies greater than 20 keV. In this work, we sent several samples for implantation spanning these ranges, as well as at 10 keV, to attempt to position the vacancies closer to the surface of the SiC to have vacancies in regions of highest electric field. The ion implantations were simulated using the SUSPRE code to estimate the doping and damage profiles through the depth of the material, and are shown in Figure 7 as an example with a dose of 10^{12} cm^{-2} and energies of 10, 20, and 100 keV. According to the simulations and prior to annealing the peak concentration of ^{12}C is at 20.5, 41.3, and 188 nm. According to the simulations at this dose, a high level of disorder is created. Ion implants were made at Innovion Corporation according to the split in Table 1. For each wafer, samples were collected of 4 and 6H and silicon control was mounted by taping the corners with polyimide tape, avoiding contact with the center 10 mm of the samples. After implantation, the samples were processed according the flow in Figure 4 in a class 100 clean room at the nano3 facilities at UC San Diego. Figure 8 shows the complete process flow for the construction of the devices starting from silicon carbide wafers, dicing, surface protection, ion implantation and anneal, as well as formation of the ITO electrodes by lift-off.
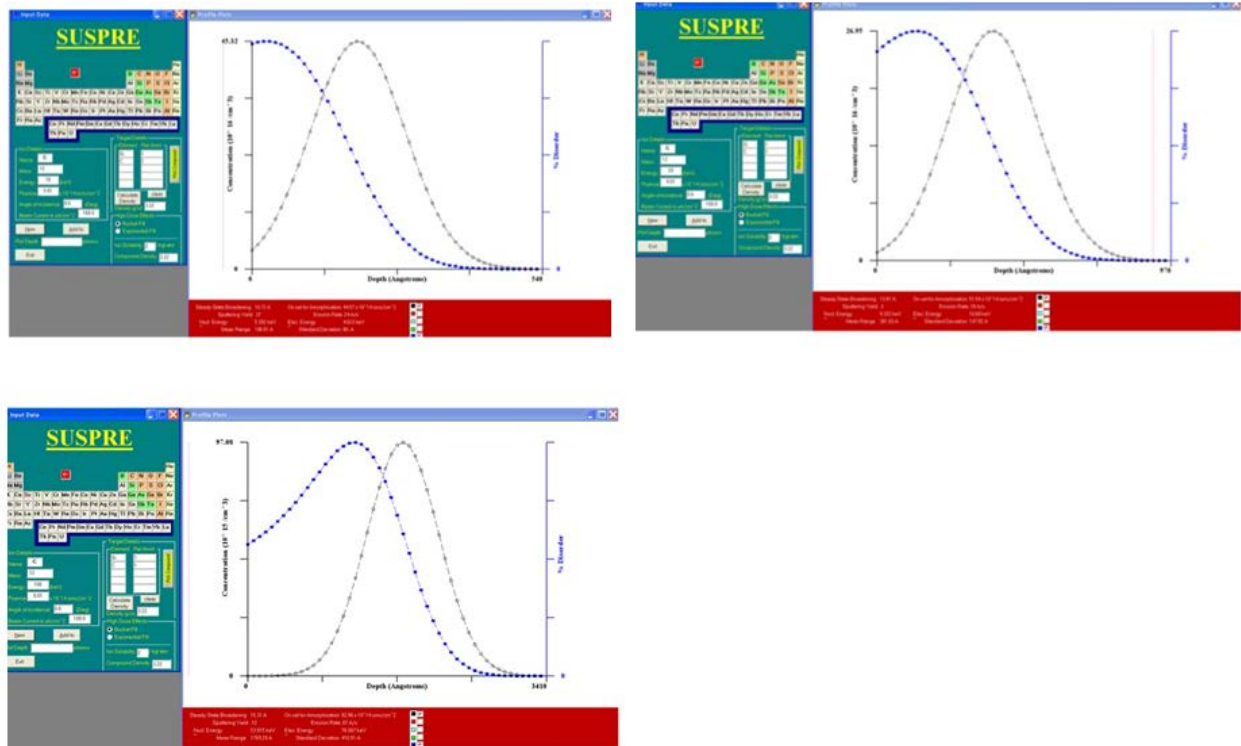
Figure 7. Ion implantation simulations of ^{12}C in silicon carbide. Simulations are made spanning experimental conditions of 10^{11} to 10^{13}-cm^{-2} dose and 10 to 200 keV. At high dose, disorder induced is significantly greater and may favor different final arrangement of the ions in the host crystal.

Table 1. Comparison of wafer numbers, species, dose, and energy for 4H SiC, 6H SiC, Si samples.

Wafer #	Species	Dose (cm^{-2})	Energy (keV)	Samples
1	^{12}C	10^{11}	200	4H SiC, 6H SiC, Si
2	^{12}C	10^{12}	200	4H SiC, 6H SiC, Si
3	^{12}C	10^{13}	200	4H SiC, 6H SiC, Si
4	^{12}C	10^{11}	50	4H SiC, 6H SiC, Si
5	^{12}C	10^{12}	50	4H SiC, 6H SiC, Si
6	^{12}C	10^{13}	50	4H SiC, 6H SiC, Si
7	^{12}C	10^{11}	20	4H SiC, 6H SiC, Si
8	^{12}C	10^{12}	20	4H SiC, 6H SiC, Si
9	^{12}C	10^{13}	20	4H SiC, 6H SiC, Si
10	^{12}C	10^{11}	10	4H SiC, 6H SiC, Si
11	^{12}C	10^{12}	10	4H SiC, 6H SiC, Si
12	^{12}C	10^{13}	10	4H SiC, 6H SiC, Si

Figure 8. Complete process flow for the construction of the devices starting from silicon carbide wafers, dicing, surface protection, ion implantation and anneal, as well as formation of the ITO electrodes by lift-off.
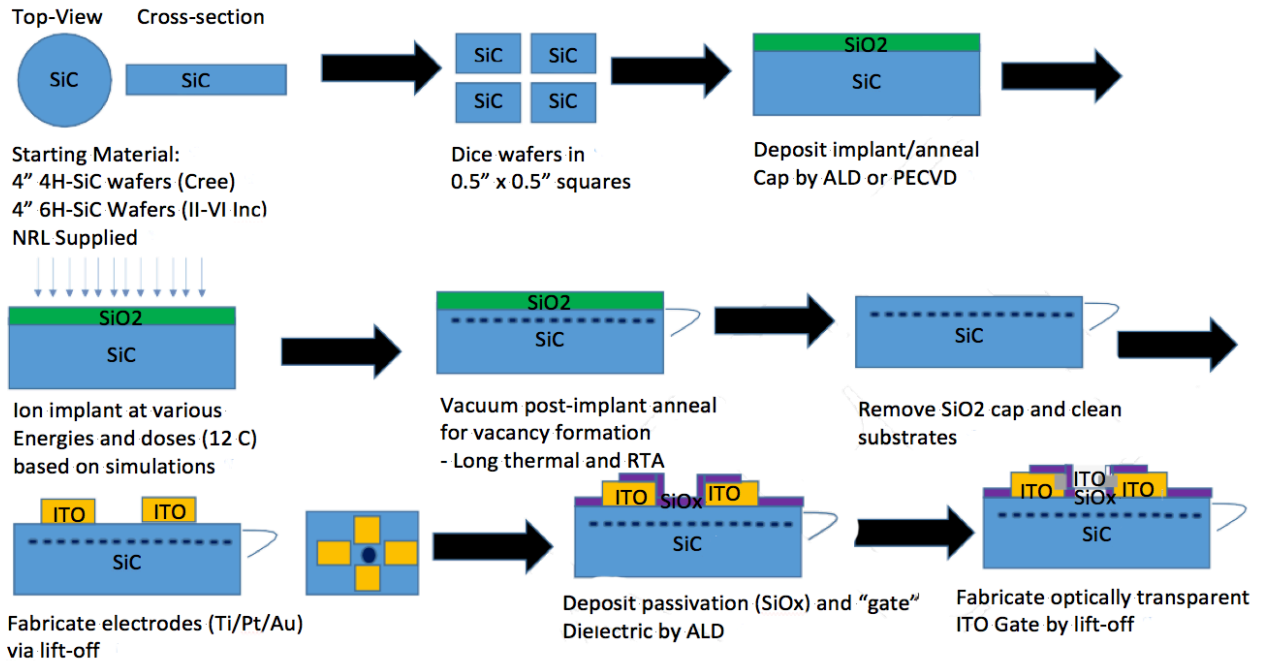
Thermal annealing was done at 1000 ^{o}C for 30 min with a ULVAC MILA-3000 Mililamp annealer under low-vacuum conditions. The thermal anneal is used to produce vacancies with a large percentage of vacancies that are suitable for use as qubits (i.e., silicon vacancies, and divacancies). Following annealing photolithography was done to define lift-off regions for deposition of the electrodes. The mask contains field-effect device structures in a ground-signal-ground (G-S-G) configuration and 150-µm separation. The "channel" length is varied on the mask ranging from 200 to 2 µm. Photolithography is completed with a MA6 mask aligner. After lithography, a dilute H_2O:HF (1:50) etch is done to etch the SiO_x in the contact regions. After etch deposition of ITO occurs by RF sputtering at 200 W in argon. After sputtering lift-off is done in acetone with ultrasonic agitation, the final product is shown in Figure 9 shows several devices and noting three regions where photoluminescence measurements are taken at PL_a, PL_b, and PL_c.
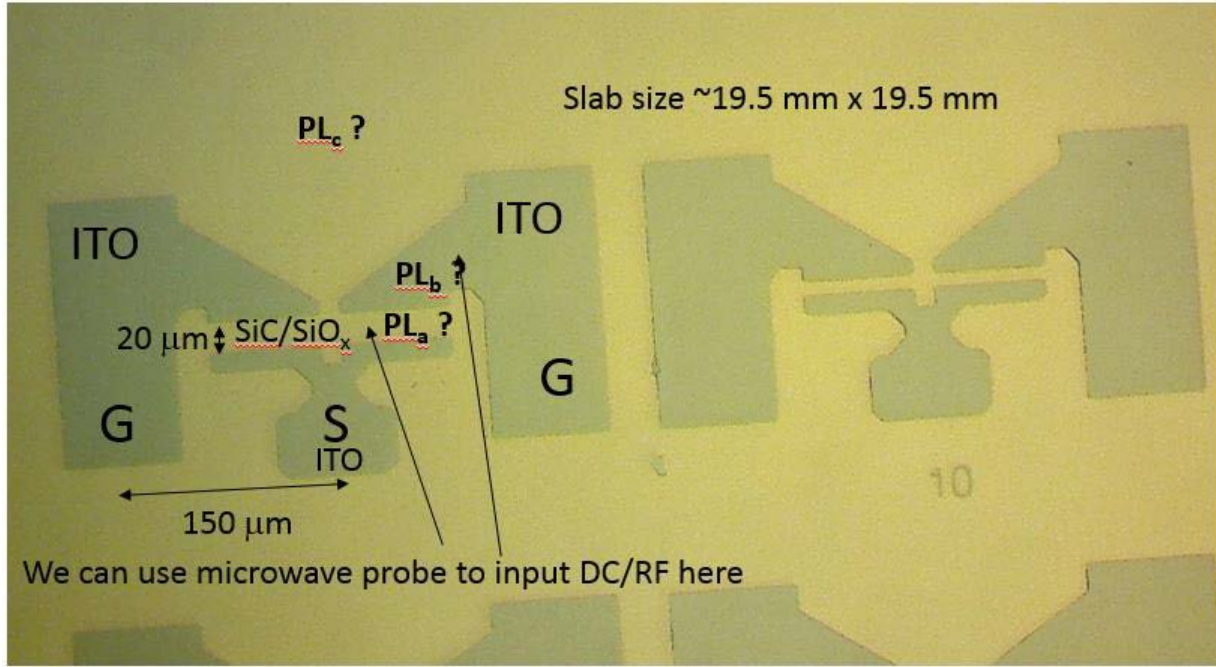
Figure 9. Top-down optical micrograph of a representative completed device showing the regions A, B, C where PL is measured. The layout used is in a G-S-G configuration spaced by 150 μm suitable for direct microwave input via probes. The slab size is 19.5 x 19.5 mm as determined by the dicing geometry.

6. SCANNING PHOTOLUMINESCENCE MEASUREMENTS

Scanning photoluminescence (PL) measurements are completed on both 4- and 6H-SiC samples at room temperature using an AIST-NT Inc. Confocal Raman/Atomic Force Microscopy (AFM) system with a laser excitation source of 785 nm, a Horiba™ iHR320 imaging spectrometer, and a Horiba™ Syncerity CCD camera thermoelectrically cooled to -50 °C with a Hamamatsu™ (S11510) near-infrared (IR) image sensor. The samples measured include both non-implanted and ^{12}C implanted 4 - and 6H-SiC with energies ranging from 20 to 50 keV and doses ranging from $10^{12\text{-}13}$. Measurements were also conducted on three different regions of the device to examine the effect of an indium tin oxide (ITO) film on the excitation and transmission of SiC PL.

Figure 10 shows the scanning PL measurement of the device channel region, PL_a for a 6H-SiC device implanted at 50 keV, and a dose of 10^{13}. Figure 10(b) shows a PL image of the scanned region where the color of each data point is assigned based on the area-under-the-curve (AUC) spanned by the green markers in Figure 10(c). The region is a 30-μm by 30-μm square and the spectra were acquired every 500-nm with an acquisition time of 100 ms using a 30-mW excitation at 785 nm. The blue and red spectra are the average spectra of the spectra encompassed by the blue and red regions (Figure 10(b)), respectively. The blue region corresponds to 6H-SiC/SiOx within the device channel and the red region corresponds to 6H-SiC/ITO/SiOx. The broad PL peak in Figure 9(b) spanning 825 to 1050 nm is suggestive of silicon vacancy defects in 6H-SiC. As these measurements were completed at room temperature, the PL shows a broad phonon sideband. To lessen the effect of electron-phonon coupling and to observe the sharp zero phonon line transitions of the defects, the device must be cooled. Additionally, small peaks corresponding to the tangential and longitudinal

optical modes (TO, LO, respectively) of 6H-SiC are present
($\approx$830 to 850 nm). The suggests that ITO has minimal impact on the transmission of the PL as confirmed by similar PL intensities and presence of 6H-SiC Raman peaks in the 6H-SiC/SiO$_x$ and 6H-SiC/ITO/SiOx regions.
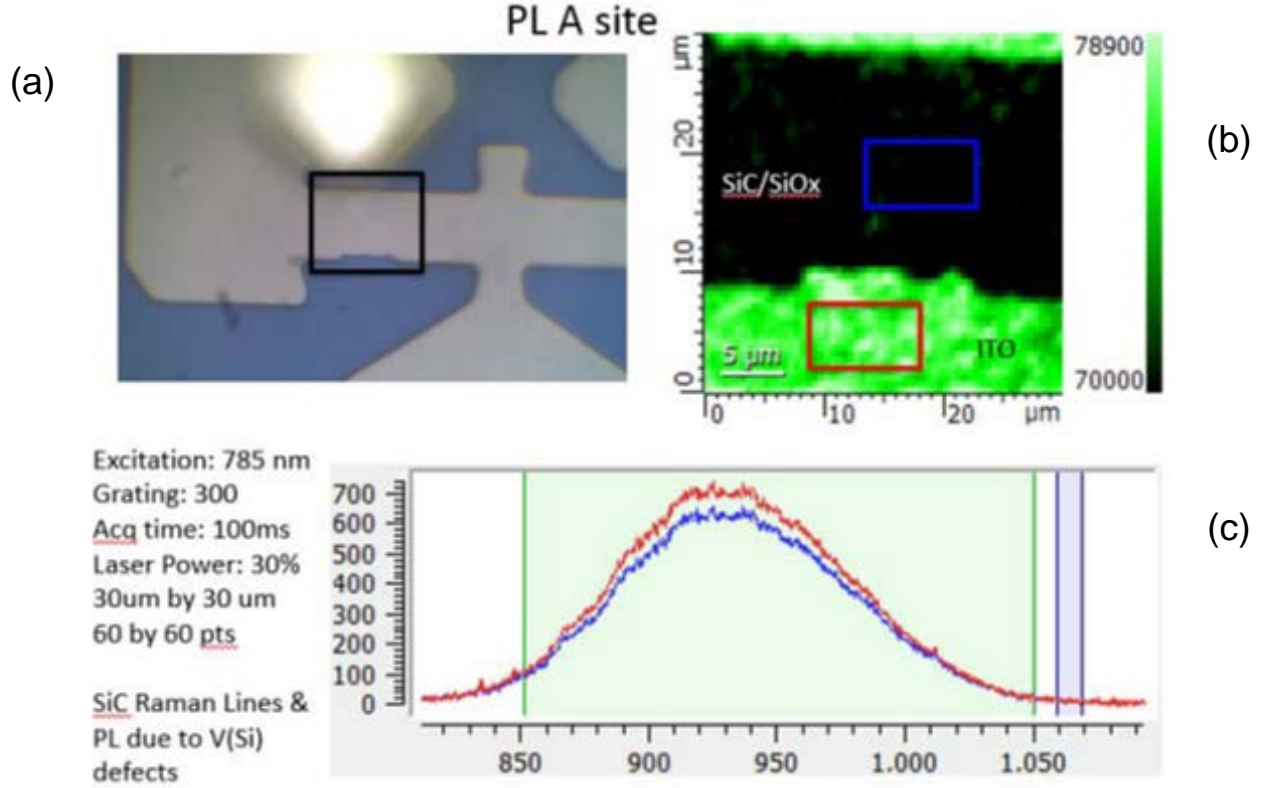

Figure 10. Microscope image of device (a). Black rectangle corresponds to scanned region (b). Photoluminescence image of scanned region. Each data point maps to a collected spectrum. The color scale corresponds to integration of the spectrum between the green markers. The blue and red rectangles encompass regions that correspond to 6H-SiC/SiOx and 6H-SiC/ITO/SiOx, respectively. (c) Averaged spectra of the 6H-SiC/SiOx (blue) and 6H-SiC/ITO/SiOx (red).

Figure 11 shows the scanning PL measurement of the ITO electrode region, PL$_B$, for a 6H-SiC device implanted at 50 keV and a dose of 10^{13}. Figure 11(a) shows a PL image of the scanned region where the color of each data point is assigned based on the area-under-the-curve (AUC) spanned by the green markers in Figure 11(b). The region is a 30 by 20 μm and the spectra were acquired every 500-nm with an acquisition time of 100 ms using a 30-mW excitation at 785 nm. The blue and red spectra are the average spectra of the spectra encompassed by the blue and red regions in Figure 11(a), respectively. Both the blue and the red region corresponds to 6H-SiC/ITO/SiOx. The spectra in Figure 11(b) correspond closely with the spectra in Figure 10(a), as the ITO film appears to have minimal impact on observing the PL of 6H-SiC.

(a)

PL B site

Excitation: 785 nm
Grating: 300
Acq time: 100ms
Laser Power: 30%
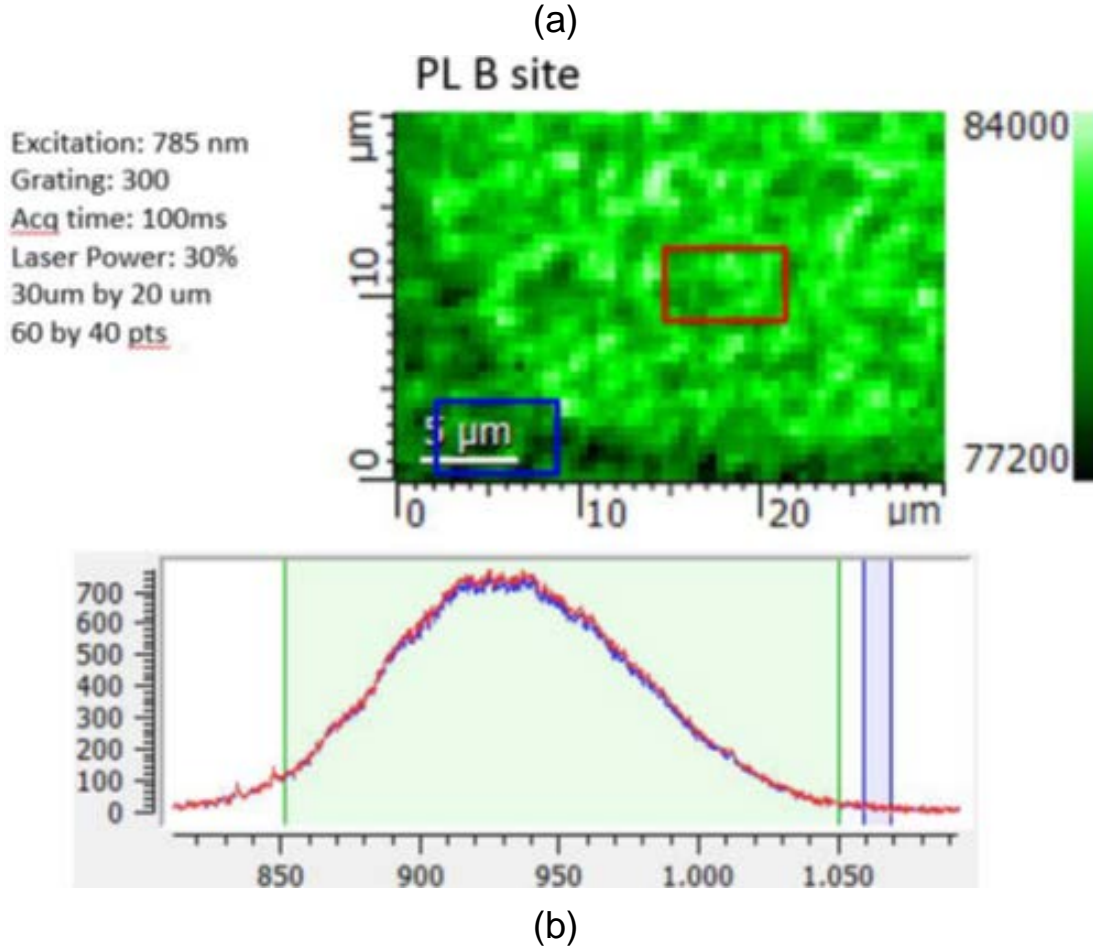30um by 20 um
60 by 40 pts

(b)

Figure 11. (a) PL image in the PLB region, (b) averaged spectra of the data points within the blue and red regions in (a).

Figure 12 shows the scanning PL measurement of the 6H-SiC/SiO$_x$ region away from the device, PLC, implanted at 50 keV and a dose of 10^{13}. Figure 12(a) shows a PL image of the scanned region where the color of each data point is assigned based on the maximum peak intensity of the collected spectra. The region is a 20 by 20 μm and the spectra were acquired every 500 nm with an acquisition time of 100 ms using a 30-mW excitation at 785 nm. Figure 12(b) shows the average spectrum of the entire region. Comparing the spectra of Figures 10(c), 11(b), and 12(b) demonstrates that the ITO and SiOx films have minimal impact on observing the PL of 6H-SiC and that the PL is nearly uniform between different regions of the sample.
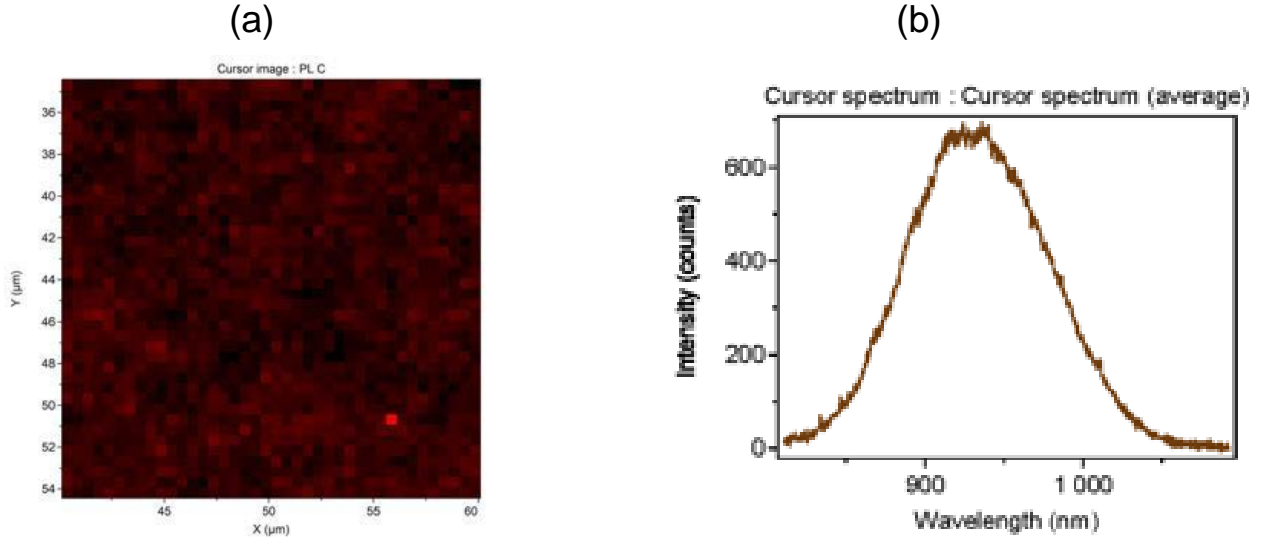
Figure 12. (a) PL image in the PL_C region, (b) averaged spectra of the data points in entire scanned region.

To confirm the effect of energy and dose in introducing defects in 6H-SiC, the PL measurements were conducted on three samples. These samples included unprocessed 6H-SiC, 6H-SiC implanted at 20 keV with dose of 10^{12}, and 6H-SiC implanted at 50 keV with dose of 10^{13}. The samples were measured using a 785-nm excitation at 100 mW. The average spectra were acquired with an acquisition time of 1 sec and 10 accumulations, and were normalized with respect to the 2nd TO peak of 6H-SiC. Figure 13 shows the average spectra of these measurements. With increasing dose and energy, the PL intensity increases indicative of increased number of defects in 6H-SiC.
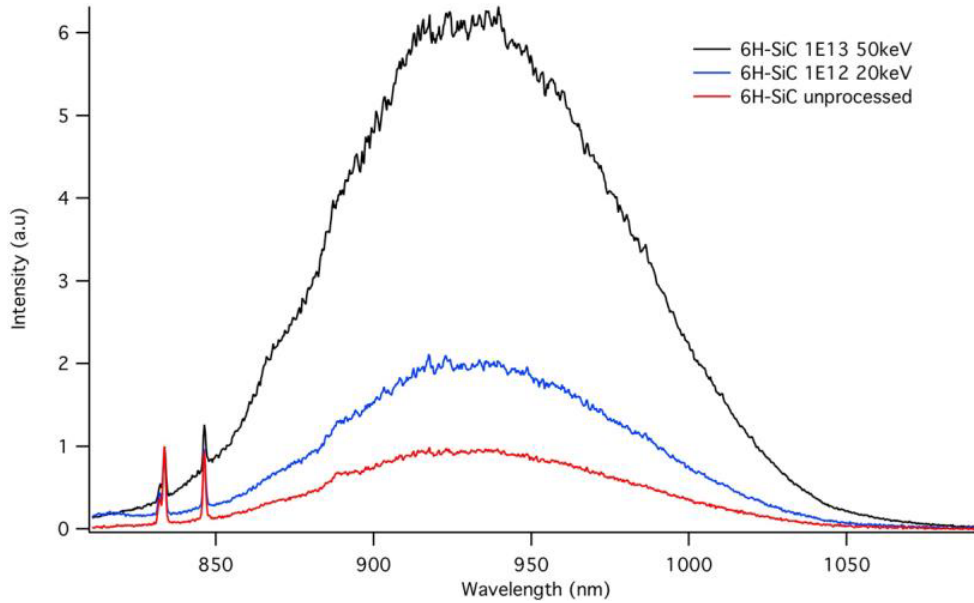

Figure 13. Spectra of 6H-SiC samples with varying implantation energies and doses normalized with respect to the 2nd TO Raman peak of 6H-SiC.

To estimate the quantity of photon emitting defects within the excitation volume, the PL of an implanted 6H-SiC sample (energy: 50 keV; dose: 10^{13}) was measured at a series of laser powers. Figure 14 shows the counts per second (cps) of the PL laser power from 0 to 100 mW. The data was fit to the equation $f(x) = a/(1+(b/x))$, where "a" corresponds to the cps when all emitters within the volume are saturated and "b" corresponds the laser power to achieve half of the saturated emission. Using an estimated 10^4 cps (Fuchs et al., 2011) for a single emitter, the estimated emitters within the excitation volume is ≈300. By varying the dose and energy of implantation, it may be possible to the decrease the number of emitting defects to achieve devices with single defects. Figure 14 shows a PL emission versus laser power for a 6" H-SiC sample.
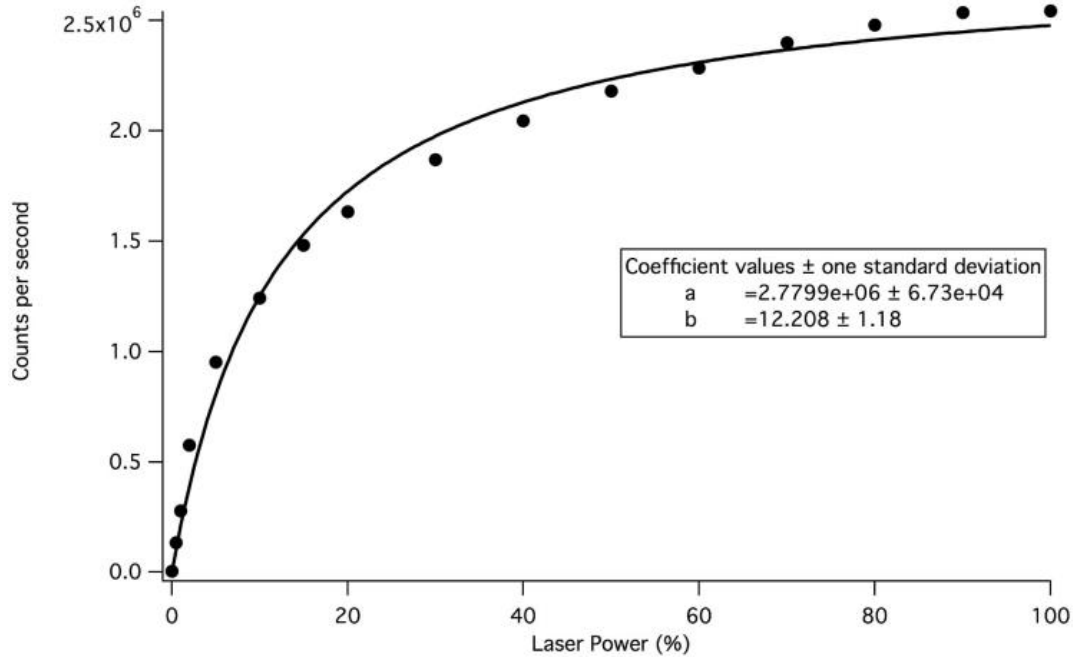

Figure 14. PL emission versus laser power for 6" H-SiC sample implanted at 50 keV and dose of 10^{13}. The data is fitted to $f(x) = a/(1+(b/x))$, where "a" corresponds to the emission when all emitters within the volume are saturated and "b" corresponds the laser power to achieve half of the saturated emission.

7. SPECTROSCOPY PROGRESS

An optical table was installed in the SSC Pacific Coastal and Estuarine Research Federation (CERF) lab and components have been procured to perform spectroscopy measurements on the silicon carbide qubits. The goal of the spectroscopy is to perform optically detected magnetic resonance measurements as well spin flip/rotation operations to evaluate the coherence times as well as toward demonstration of entanglement. The two photos in Figure 15 show the optical setup at SSC Pacific integrating free-space and fiber-optic lasers, optics for collected PL spectra and spectrometers.
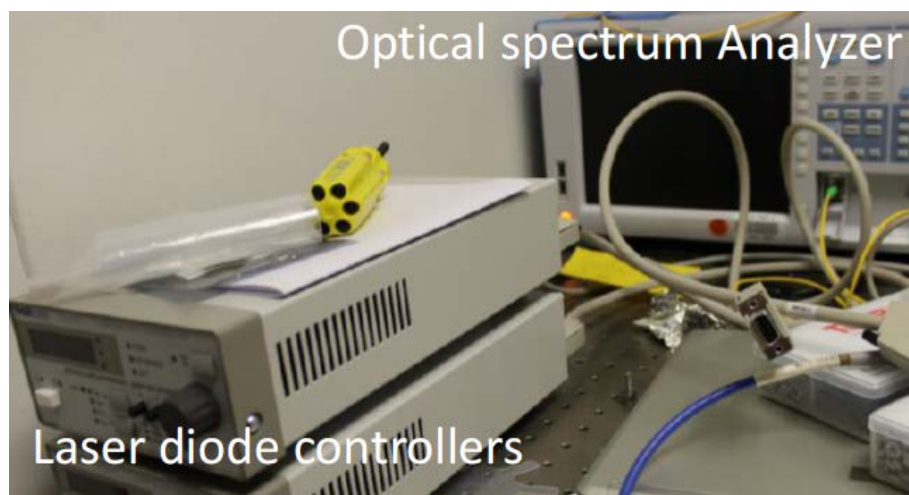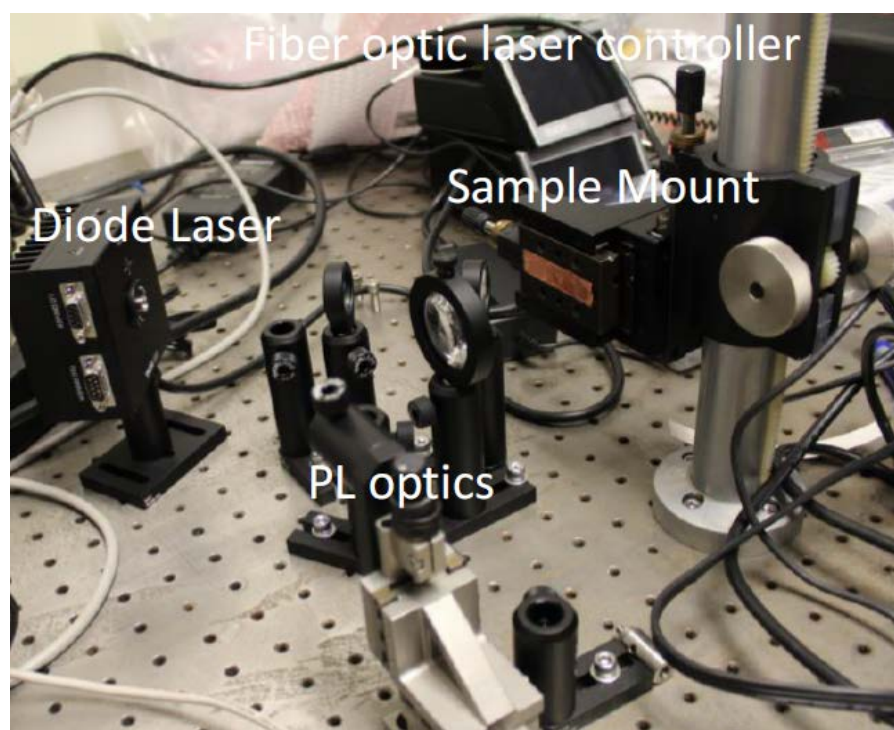
Figure 15. Optical setup at SSC Pacific integrating free-space and fiber-optic lasers, optics for collected PL spectra, and spectrometers.

8. PULSED MICROWAVE/RF CONTROL

Microwave/RF control methods were developed using state-of-the-art equipment in the CERF lab. These methods were developed in support of an Office of Naval Research (ONR) funded in-house laboratory initiative and are applicable to use for silicon carbide qubits. State-of-the-art cryogenic amplifiers and filters are used to obtain the highest quality microwave and RF pulses for control of the nuclear and electronic spin states of the silicon carbide vacancy qubits. An electronic rack and MATLAB® Simulink framework were developed for production of these pulses, which will be used with proper timing in conjunction with the optical spectroscopy. Figure 16 shows the microwave/RF pulsing equipment.
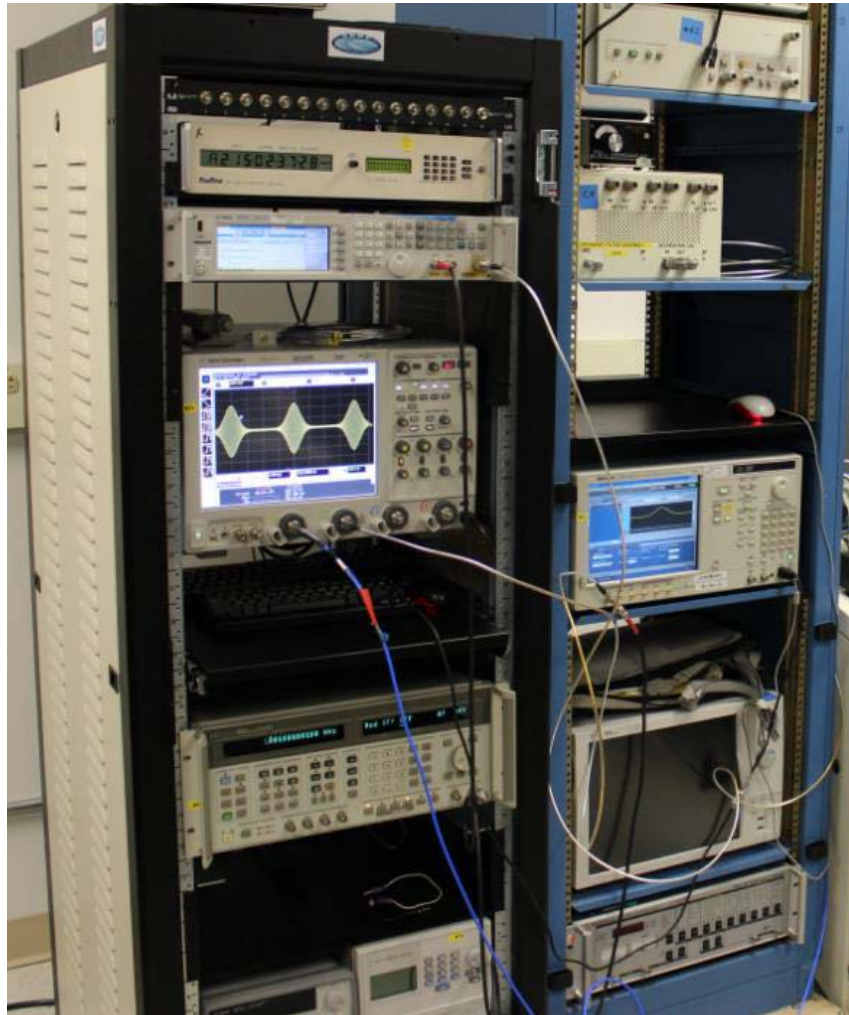

Figure 16. Microwave/RF pulsing equipment to be used for qubit control in conjunction with the optical control.

9. PHOTONIC CIRCUIT INTEGRATION PROGRESS

The silicon carbide qubit devices were constructed in a layout that permits easy integration of photonic components on chip. It is known that the processes of forming structures such as photonic crystals and waveguides with silicon carbide material may be detrimental to the qubits due to requirement of plasma etching to form silicon carbide structures. For this reason, alternate materials (e.g., silicon nitride) that can be used for photonic crystals and waveguides that can deposited gently after formation of the qubits are in development. Discussions are being held between NRL and SSC Pacific researchers about the possibility of attempting the experiment during the second year of this project.

10. TOWARDS SINGLE DEFECT AND PHOTON LEVELS

The physics of quantum entanglement requires performing qubit and quantum memory operation on single photon routes for getting to the single photon level are being pursued. These routes include looking into processes for construction of devices that integrate single defects that can be probed, upgrades for the cryo-magneto-optical probe station to integrate scanning confocal capability, development of photonic crystal structures for increasing the detection sensitivity and examining routes for integration of single photon detectors, and ultra-faster lasers. In alignment with this effort, discussions are underway with industry who develop several such tools.

11. ENTANGLEMENT ARCHITECTURE AND DEMONSTRATION PREPERATION

Discussions and review of entanglement architectures are occurring, particularly focusing on prior success using diamond quantum memories as well as the more recent work on silicon carbide from the University of Chicago. In preparation, a fiber link was established between two points on the SSC Pacific campus to facilitate quantum measurements and sending entanglement, one at the CERF lab and the other the advanced photonics technology lab where a tunable femto second laser is installed. One entanglement is established, then studies of long distance entanglement will be made. Concurrently, Cooperative Research and Development Agreements (CRADAs) are being establishing between SSC Pacific and industrial partners that develop quantum entanglement equipment. The goal is to investigate quantum communications though integration of industrial technologies with the quantum memories. Advanced protocols such as BB84 and Ekert 91 are being looked into on how to implement with solid state qubits. Figure 17 locations used for experiments sending entanglement across long distances using fiber.
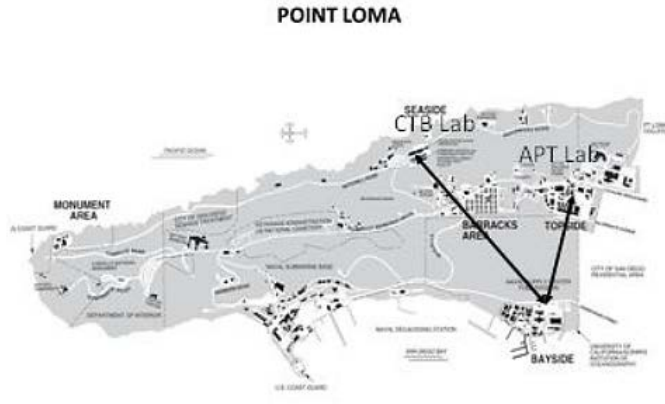
Figure 17. Fiber-optic photonic link port A, and connected a few kilometers away at point B on campus, to be used for experiments in sending entanglement across long distances via fiber.

12. SUMMARY

In summary, this technical report summarizes progress of the SSC Pacific–NRL collaboration in support of the OSD Quantum Science and Engineering Program. In particular, performance was met in fabrication of the silicon carbide qubit in line with the overall goals of the program. Significant progress is also being made towards quantum entanglement demonstrations and is summarized to include photoluminescence, spectroscopy, RF/microwave control, photonic integration, and single photon detection. The work has benefits from leveraging concurrent projects with aligned goals.

BLIOGRAPHY

Aharonovich, I., D. Englund, and M. Toth. 2016. "Solid-state Single-photon Emitters," *Nature Photonics 10*(10):631–641. DOI: https://doi.org/10.1038/nphoton.2016.186

Christle, D. J., A. L. Falk, P. Andrich, P. V. Klimov, J. U. Hassan, N. T. Son, E. Janzén, T. Ohshima, and D. D. Awschalom. 2015. "Isolated Electron Spins in Silicon Carbide with Millisecond Coherence Times," *Nature Materials 14*(2):160–163. DOI: https://doi.org/10.1038/nmat4144

Carter, S. G., Ö. O. Soykal, P. Dev, S. E. Economou, and E. R. Glaser. 2015. "Spin Coherence and Echo Modulation of the Silicon Vacancy in 4 H− SiC at Room Temperature," *Physical Review B 92*(16):161202. DOI: https://doi.org/10.1103/PhysRevB.92.161202

Falk, A. L., P. V. Klimov, B. B. Buckley, V. Ivády, I. A. Abrikosov, G. Calusine, W. F. Koehl, Á. Gali, and D. D. Awschalom. 2014. "Electrically and Mechanically Tunable Electron Spins in Silicon Carbide Color Centers," *Physical Review Letters 112*(18):187601. DOI: https://doi.org/10.1103/PhysRevLett.112.187601

Falk, A. L., P. V. Klimov, V. Ivády, K. Szász, D. J. Christle, W. F. Koehl, A. Gali, and D. D. Awschalom. 2015. "Optical Polarization of Nuclear Spins in Silicon Carbide," *Physical Review Letters 2*(24):247603. DOI: https://doi.org/10.1103/PhysRevLett.114.247603

Fisher, K. A. G., D. England, J. W. Maclean, P. Bustard, R. Lausten, K. J. Resch, and B. Sussman. 2015. "Storage and Retrieval of Ultrafast Single Photons Using a Room-temperature Diamond Quantum Memory." *Proceedings of Conference on Lasers and Electro-Optics: QELS_Fundamental Science 2015* (paper FTh4B-5). 10–15 May, San Jose, CA. DOI: https://doi.org/10.1364/CLEO_QELS.2015.FTh4B.5

Fuchs, G. D., G. Burkard, P. V. Klimov, and D. D. Awschalom. 2011. "A Quantum Memory Intrinsic to Single Nitrogen-vacancy Centres in Diamond," *Nature Physics 7*(10):789–793.

Gomi, T., S. Tomizawa, K. Ohashi, K. M. Itoh, J. Ishi-Hayase, H. Watanabe, H. Umezawa, and S. Shikata. 2013. "Position and Density Control of Nitrogen-vacancy Centers in Diamond Using Micropatterned Substrate for Chemical Vapor Deposition." *Proceedings of Conference on Lasers and Electro-Optics/Pacific Rim* (paper WI1_3). 30 June to 4 July, Kyoto, Japan. Available online at https://www.osapublishing.org/abstract.cfm?uri=CLEOPR-2013-WI1_3. Accessed on June 30, 2017.

Hensen, B., H. Bernien, A. E. Dréau, A. Reiserer, N. Kalb, M. S. Blok, J. Ruitenberg R. F. L. Vermeulen, R. N. Schouten, C. Abellán, W. Amaya, V. Pruneri, M. W. Mitchell, M. Markham, D. J. Twitchen, D. Elkouss, S. Wehner, T. H. Taminiau, and R. Hanson. 2015. "Loophole-free Bell Inequality Violation Using Electron Spins Separated by 1.3 km," *Nature 526*(7575):682–686. DOI: https://doi.org/doi:10.1038/nature15759

Klimov, P. V., A. L. Falk, D. J. Christle, V. V. Dobrovitski, and D. D. Awschalom. 2015. "Quantum Entanglement at Ambient Conditions in a Macroscopic Solid-state Spin Ensemble," *Science Advances 1*(10):e1501015. DOI: https://doi.org/ 10.1126/sciadv.1501015

Klimov, P. V., A. L. Falk, B. B. Buckley, and D. D. Awschalom. 2014. "Electrically Driven Spin Resonance in Silicon Carbide Color Centers," *Physical Review Letters 112*(8):087601. DOI: https://doi.org/10.1103/PhysRevLett.112.087601

Lee, S. W., S. I. Vlaskina, V. I. Vlaskin, I. V. Zaharchenko, V. A. Gubanov, G. N. Mishinova, G. S. Svechnikov, V. E. Rodionov, and S. A. Podlasov. 2010. "Silicon Carbide Defects and Luminescence Centers in Current Heated 6H-SiC," *Semiconductor Physics Quantum Electronics & Optoelectronics 13*(1):24–29.

Ohashi, K., T. Rosskopf, H. Watanabe, M. Loretz, Y. Tao, R. Hauert, S. Tomizawa, T. Ishikawam J. Ishihayase, S. Shikata, C. L. Degent, and K. M. Itoh. 2013. "Negatively Charged Nitrogen-vacancy Centers in a 5 nm Thin ^{12}C Diamond Film," *Nano Letters 13*(10):4733–4738. DOI: https://doi.org/10.1021/nl402286v

Schneider, J., H. D. Müller, K. Maier, W. Wilkening, F. Fuchs, A. Dörnen, S. Leibenzeder, and R. Stein. 1990. "Infrared Spectra and Electron Spin Resonance of Vanadium Deep Level Impurities in Silicon Carbide," *Applied Physics Letters 56*(12):1184–1186. DOI: http://dx.doi.org/10.1062/1.102555

Simmons, S., R. M. Brown, H. Riemann, N. V. Abrosimov, P. Becker, H. Pohl, M. L. W. Thewalt, K. M. Itoh, and J. J. L. Morton. 2011. "Entanglement in a Solid-state Spin Ensemble," *Nature 470*:69–72. DOI: https://doi.org/ 10.1038/nature09696

Soykal, Ö. O., and T. L. Reinecke. 2017. "Quantum Metrology with a Single Spin-3/2 Defect in Silicon Carbide," *Physical Review B 95*(8):081405. DOI: https://doi.org/10.1103/PhysRevB.95.081405

Soykal, Ö. O., P. Dev, and S. E. Economou. 2016. "Silicon Vacancy Center in 4 H-SiC: Electronic Structure and Spin-photon Interfaces," *Physical Review B 93*(8):081207. DOI: https://doi.org/10.1103/PhysRevB.93.081207

Vrijen, R., E. Yablonovitch, K. Wang, H. W. Jiang, A. Balandin, V. Roychowdhury, T. Mor, and D. DiVincenzo. 2000. "Electron-spin-resonance Transistors for Quantum Computing in Silicon-germanium Heterostructures," *Physical Review A 62*(1):012306. DOI: https://doi.org/10.1103/PhysRevA.62.012306

REPORT DOCUMENTATION PAGE

Form Approved
OMB No. 0704-01-0188

The public reporting burden for this collection of information is estimated to average 1 hour per response, including the time for reviewing instructions, searching existing data sources, gathering and maintaining the data needed, and completing and reviewing the collection of information. Send comments regarding this burden estimate or any other aspect of this collection of information, including suggestions for reducing the burden to Department of Defense, Washington Headquarters Services Directorate for Information Operations and Reports (0704-0188), 1215 Jefferson Davis Highway, Suite 1204, Arlington VA 22202-4302. Respondents should be aware that notwithstanding any other provision of law, no person shall be subject to any penalty for failing to comply with a collection of information if it does not display a currently valid OMB control number. **PLEASE DO NOT RETURN YOUR FORM TO THE ABOVE ADDRESS.**

1. REPORT DATE *(DD-MM-YYYY)*	2. REPORT TYPE	3. DATES COVERED *(From - To)*
August 2017	Final	

4. TITLE AND SUBTITLE

Silicon Carbide Defect Qubits/Quantum Memory with Field Tuning: OSD Quantum Science and Engineering Program (QSEP)

5a. CONTRACT NUMBER

5b. GRANT NUMBER

5c. PROGRAM ELEMENT NUMBER

6. AUTHORS

Osama Nayfeh, Brad Liu, Vincent Dinh, Carlos Torres, Anna Leese de Escobar **SSC Pacific**

Mark Lasher, Sanja Zlatanovic, Bradley Davidson, Patrick Sims, Brian Higa

Lance Lerum, Hector Romero **NREI Program**

Mohammed Fahem **SDSU Research Foundation**

Hunter Banks, Sam G. Carter, D. Kurt Gaskill, Thomas L. Reinecke **NRL**

5d. PROJECT NUMBER

5e. TASK NUMBER

5f. WORK UNIT NUMBER

7. PERFORMING ORGANIZATION NAME(S) AND ADDRESS(ES)

SSC Pacific
53560 Hull Street
San Diego, CA 92152–5001

8. PERFORMING ORGANIZATION REPORT NUMBER

TR 3073

9. SPONSORING/MONITORING AGENCY NAME(S) AND ADDRESS(ES)

Office of Secretary of Defense-Naval Research Lab
Quantum Science and Engineering Program
4555 Overlook Ave., SW
Washington, DC 20375

10. SPONSOR/MONITOR'S ACRONYM(S)
NRL

11. SPONSOR/MONITOR'S REPORT NUMBER(S)

12. DISTRIBUTION/AVAILABILITY STATEMENT

Approved for public release.

13. SUPPLEMENTARY NOTES

This is work of the United States Government and therefore is not copyrighted. This work may be copied and disseminated without restriction.

14. ABSTRACT

Collaboration between Space and Naval Warfare Systems Center Pacific (SSC Pacific) and the Naval Research Lab (NRL) was initiated in 2015 and 2016 as part of the OSD Quantum Science and Engineering Program (QSEP). The collaboration's topic is to examine the effect of an electric-field on silicon carbide qubits as a unique contribution, as well as a general benefit in increasing knowledge in the quantum information field and working towards supporting demonstrations of quantum entanglement based on these qubits and quantum memories developed out of the silicon carbide system and other systems as necessary through the QSEP program. This year's highlights included successful completion of a novel process flow for the construction of the tunable qubits, measurements of the optical emission from the devices, simulations of the tuning process, and progress for experimental validation of the concepts and for supporting entanglement demonstrations. A patent disclosure was filed on the concept of tunable silicon carbide qubits as well as a conference abstract was accepted to the SPIE 2017 nanoscience + engineering conference for consideration in the quantum photonic devices section.

15. SUBJECT TERMS

Quantum Science and Engineering Program (QSEP); electric-field; silicon carbide; qubits; quantum; quantum entanglement; quantum memories; tunable qubits; optical emission; tuning process; entanglement demonstrations; quantum photonic devices; photoluminescence measurements; spectroscopy; photonic circuit;

16. SECURITY CLASSIFICATION OF:			17. LIMITATION OF ABSTRACT	18. NUMBER OF PAGES	19a. NAME OF RESPONSIBLE PERSON
a. REPORT	b. ABSTRACT	c. THIS PAGE			Osama Neyfeh
U	U	U	U	31	**19B. TELEPHONE NUMBER** *(Include area code)* (619) 553-2770

Standard Form 298 (Rev. 8/98)
Prescribed by ANSI Std. Z39.18

INITIAL DISTRIBUTION

Approved for public release.

SSC Pacific
San Diego, CA 92152-5001